Geophysical Journal International

Geophys. J. Int. (2014) **196,** 432–446
Advance Access publication 2013 October 16

doi: 10.1093/gji/ggt371

Towards real-time regional earthquake simulation I: real-time moment tensor monitoring (RMT) for regional events in Taiwan

Shiann-Jong Lee,[1] Wen-Tzong Liang,[1] Hui-Wen Cheng,[2] Feng-Shan Tu,[1] Kuo-Fong Ma,[2] Hiroshi Tsuruoka,[3] Hitoshi Kawakatsu,[3] Bor-Shouh Huang[1] and Chun-Chi Liu[1]

[1] *Institute of Earth Sciences, Academia Sinica, Taipei* 11529*, Taiwan. E-mail: sjlee@earth.sinica.edu.tw*
[2] *Institute of Geophysics, National Central University, Jhongli, Taoyuan* 32001*, Taiwan*
[3] *Earthquake Research Institute, University of Tokyo,* 1-1-1 *Yayoi, Bunkyo-ku, Tokyo* 1130032*, Japan*

Accepted 2013 September 13. Received 2013 September 12; in original form 2013 June 17

SUMMARY

We have developed a real-time moment tensor monitoring system (RMT) which takes advantage of a grid-based moment tensor inversion technique and real-time broad-band seismic recordings to automatically monitor earthquake activities in the vicinity of Taiwan. The centroid moment tensor (CMT) inversion technique and a grid search scheme are applied to obtain the information of earthquake source parameters, including the event origin time, hypocentral location, moment magnitude and focal mechanism. All of these source parameters can be determined simultaneously within 117 s after the occurrence of an earthquake. The monitoring area involves the entire Taiwan Island and the offshore region, which covers the area of 119.3°E to 123.0°E and 21.0°N to 26.0°N, with a depth from 6 to 136 km. A 3-D grid system is implemented in the monitoring area with a uniform horizontal interval of 0.1° and a vertical interval of 10 km. The inversion procedure is based on a 1-D Green's function database calculated by the frequency–wavenumber (*fk*) method. We compare our results with the Central Weather Bureau (CWB) catalogue data for earthquakes occurred between 2010 and 2012. The average differences between event origin time and hypocentral location are less than 2 s and 10 km, respectively. The focal mechanisms determined by RMT are also comparable with the Broadband Array in Taiwan for Seismology (BATS) CMT solutions. These results indicate that the RMT system is realizable and efficient to monitor local seismic activities. In addition, the time needed to obtain all the point source parameters is reduced substantially compared to routine earthquake reports. By connecting RMT with a real-time online earthquake simulation (ROS) system, all the source parameters will be forwarded to the ROS to make the real-time earthquake simulation feasible. The RMT has operated offline (2010–2011) and online (since January 2012 to present) at the Institute of Earth Sciences (IES), Academia Sinica (http://rmt.earth.sinica.edu.tw). The long-term goal of this system is to provide real-time source information for rapid seismic hazard assessment during large earthquakes.

Key words: Time-series analysis; Inverse theory; Earthquake source observations; Seismic monitoring and test-ban treaty verification; Computational seismology.

1 INTRODUCTION

The centroid moment tensor (CMT) inversion is one of the common ways to retrieve point source information for moderate-to-large earthquakes. The CMT is also a very good representation of the fault rupture mechanism during an earthquake. The definition of CMT was first proposed by Backus & Mulcahy (1976). Successful development of CMT inversion technique has enabled the automated determination procedure to examine earthquakes worldwide, for example, the Havard CMT (Dziewonski *et al*. 1981), the USGS CMT (Sipkin 1982), the ERI AUTOCMT (Kawakatsu 1995) and the Global CMT project (http://www.globalcmt.org/; Ekström *et al*. 2012). There are also several studies which use regional waveform data to analyse CMT of local events. For example, Dreger & Helmberger (1993) used the broad-band waveforms to invert the moment tensor and focal mechanism of regional earthquakes in

the United States; Bernardi *et al*. (2004) applied the moment tensor inversion for earthquakes which occurred in the European–Mediterranean region; Fukuyama *et al*. (1998) used regional broadband seismic network data (F-net) to analyse source parameter information in Japan.

In late 1992, the Institute of Earth Sciences (IES), Academia Sinica, initiated a project to establish the Broadband Array in Taiwan for Seismology (BATS), which has paved the way for seismotectonic studies in the Taiwan region (Kao *et al*. 1998; Kao & Jian 2001). Over the past decade, the moment tensor inversion for local earthquakes has become a routine that is performed by the BATS data centre (Kao *et al*. 2002; Liang *et al*. 2003; Liang *et al*. 2004). The CMT solutions and BATS waveform data set are available online at the BATS website (http//bats.earth.sinica.edu.tw). A modified moment tensor inversion procedure from BATS is incorporated with the Central Weather Bureau (CWB) broad-band seismic network from which the corresponding CMT solution is reported for moderate-to-large earthquakes in the Taiwan region since 2005 (http://cwbsnbb.cwb.gov.tw).

Both of these routine CMT solutions require some lag time to receive the CWB rapid earthquake report (event origin time, location and local magnitude) before data preparation and performing the moment tensor inversion analysis. Usually the CWB can detect earthquakes occur in the vicinity of Taiwan within 45 s. All the source information are confirmed and then released to the public in 3–5 min. Considering the network communication time that is required for distributing the earthquake information from CWB to local server, the entire latency before further to implement the moment tensor inversion analysis can be longer. This is also a common problem in most of the automatic CMT inversion systems in the world, for example, the near–real-time MT in Greece (AUTH-solutions, Roumelioti *et al*. 2008) and the automatic regional MT in the European–Mediterranean region (Bernardi *et al*. 2004).

To solve this problem, Kawakatsu (1998) suggested a possibility of monitoring the long-period wavefield in real time using a grid-based search algorithm. Based upon this algorithm, Tsuruoka *et al*. (2009a) developed and implemented a new grid-based earthquake analysis system (GRiD MT, http://wwweic.eri.u-tokyo.ac.jp/GRiD MT/) that continuously monitors earthquake activity using broad-band seismograms. This new analysis system automatically and simultaneously determines the origin time, location and seismic moment tensor of seismic events within 3 min of their occurrence offshore of northeastern Tohoku. However, there are areas that can be improved upon with the GRiD MT, including (1) how to deal with missing data, (2) extend the monitoring area and (3) improve performance by multiple-PC processing (Tsuruoka *et al*. 2009a). Tajima *et al*. (2002) developed a similar automatic system (AMT), with 0.25° in grid space and real-time waveforms shifted forward with ∼20-s time interval, to simultaneously determine the centroid source location and seismic moment tensor for regional earthquakes that occurred in northern California. Due to the restraint of system performance, the resolutions in both event origin time and hypocentral location are required to be improved to serve the purpose of monitoring seismic events in real time. Lee *et al*. (2010) applied the grid-based moment tensor inversion technique by using a 3-D Green's functions database to analyse the detailed source parameters, including both the hypocentral location and focal mechanism, of a local earthquake that occurred near the Taipei Basin on 2004 October 23. By the use of *W*-phase and/or high-rate GPS data, the grid-based CMT inversion approach can also be applied to the large events (Duputel *et al*. 2011; Melgar *et al*. 2011). Guilhem & Dreger (2011) implemented the GRiD MT method for the Mendocino Triple Junction region, and suggested modifying the approach for characterizing large earthquakes (i.e. $M > 7$).

In this study, we develop a real-time moment tensor monitoring system, in short called RMT (http://rmt.earth.sinica.edu.tw/), to monitor seismic activity in the vicinity of Taiwan. Unlike the standard moment tensor inversion procedure, the RMT system searches the entire model space every 2 s, thus does not require *a priori* information on an earthquake's origin time and hypocentral coordinates to invert the source moment tensor. The RMT provides all the point source information automatically in real time, including event occurrence time, hypocentral location, moment magnitude, moment tensor and focal mechanism simultaneously once the earthquake is detected. The basic concept of this system is similar to the GRiD MT system recently operated in Japan (Tsuruoka *et al*. 2009a). We make several improvements to utilize the real-time BATS data flow and to deal with the missing data problem. This system uses six BATS stations in Taiwan. When one or two stations have missing data problems, the remaining stations can still provide good azimuthal coverage. Furthermore, a parallel computing technique is applied to improve system performance, which is crucial to realize real-time earthquake monitoring at the regional scale. The high seismicity rate in Taiwan and high-quality broad-band continuous waveform data provide us a good opportunity to develop these inversion techniques and test the reliability of this real-time earthquake monitoring system. In this paper, the developments and details of RMT system are presented in Section 2. Offline (2010–2011) and online (since 2012 January to present) results are shown and analysed in Section 3. In Section 4, we provide comprehensive discussions on system performance and future developments.

2 RMT DATA AND METHOD

2.1 System flowchart

The flowchart of the RMT system is shown in Fig. 1. First, the BATS database server broadcasts real-time broad-band waveforms through internet via 'Seedlink' (software developed by GEOFON Program of GFZ Potsdam, Hanka *et al*. 2000). The RMT server acquires the raw data by using 'slinktool' that is maintained by Incorporated Research Institutions for Seismology (IRIS); the data format is converted and processed on the RMT server through 'getRTsac' script (Fig. 1). Then, a parallel program named 'Parallel RMT', which is the kernel of this monitoring system to perform the moment tensor inversion and search for the best-fit solution through all virtual source points (see Fig. 2). The inversion and grid search

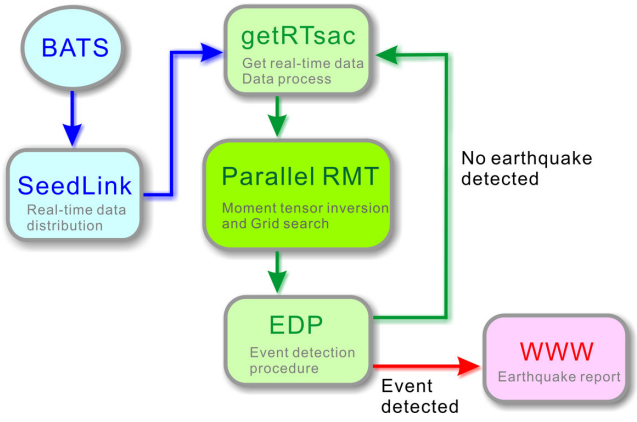

Figure 1. The flowchart of real-time moment tensor monitoring system.

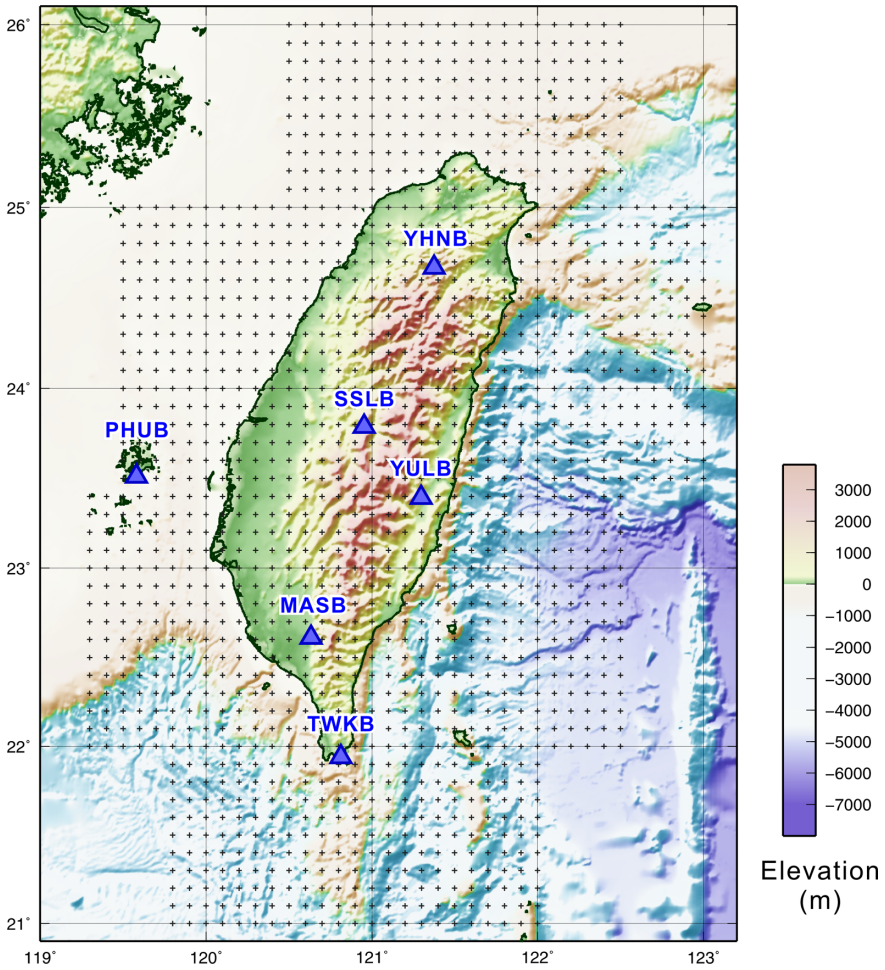

Figure 2. Distribution of virtual source gridpoints and the six BATS stations used in this study. Black crosses show the surface projection of 21 154 3-D distributed gridpoints, which covers the region from 119.3°E to 123.0°E, 21.0°N to 26.0°N and the depth from 6 to 136 km. Blue triangles are the locations of the six BATS stations used.

result is evaluated by an event-detecting procedure (EDP). If no event is detected, the system will go back to 'getRTsac' to retrieve new data. Once the earthquake is detected by the system, the RMT will announce alarms via the webpage and provide a summary of event information automatically within 2 min after the occurrence of an earthquake. All of these monitoring results will be shown on the RMT webpage in real time.

2.2 Data processing

For continuous data flow processing, the BATS database server broadcasts real-time broad-band data in seed format via 'Seedlink'. The RMT server fetches the raw data and performs a series of data-processing procedures, including converting data format from seed to SAC (Seismic Analysis Code), time synchronization, cutting the time window, applying a bandpass filter and resampling the waveform to one point per second. The time window used in the RMT is 100 s; this time window is long enough to include the first arrival and/or later phases when the seismic wave propagates from offshore to BATS stations on the island. We bandpass filtered the continuous broad-band seismogram for the frequency between 0.02 and 0.1 Hz. For this long period, low-frequency band signal, the details of localized path and structure effects can be discounted.

2.3 Inversion method

In this study, the moment tensor inversion problem is formulated in a linear form, $\mathbf{Ax} = \mathbf{b}$, where $\mathbf{A}$ is the matrix of Green's functions, $\mathbf{b}$ is the observed data vector and $\mathbf{x}$ is the solution vector of six moment tensor elements (Aki & Richards 1980). We use the singular value decomposition technique to solve this linear system of equation for the six moment tensor elements. The misfit between observed data and synthetics is assessed based on the least-square waveform misfit function (Mellman *et al*. 1975)

$$E_i = 1 - \frac{\int_0^T [f_i(t) g_i(t)]\, \mathrm{d}t}{\sqrt{\int_0^T f_i(t)^2\, \mathrm{d}t}\sqrt{\int_0^T g_i(t)^2\, \mathrm{d}t}}, \quad (1)$$

where $f_i(t)$ and $g_i(t)$ are observed and synthetic seismograms, respectively. E_i is 0 if it is a perfect fit. The advantage of this formula is that it is more sensitive to the correlation of waveforms than the absolute amplitudes (Wallace *et al*. 1981). Thus, knowing *a priori* structural details becomes less critical.

To search for the best-fit solution in all virtual gridpoints, instead of the quantity estimated E_i, a misfit reduction (MR)

$$\mathrm{MR} = (1 - E_i) \times 100\% \quad (2)$$

is used in the actual monitoring system. Because it depends on E_i, MR is an indicator of the fit between the observed waveform and

the synthetic waveform. The MR value of a perfect fit in waveform will be 100.

In addition, we considered a variance reduction (VR)

$$\mathrm{VR} = \left[1 - \frac{\int_0^T [f_i(t) - g_i(t)]^2 \mathrm{d}t}{\int_0^T f_i(t)^2 \mathrm{d}t}\right] \times 100\% \quad (3)$$

as the second indicator to evaluate the waveform fitting. From the online monitoring and offline tests, we find that the VR is too sensitive to the absolute amplitudes, especially when a large phase dominates the seismogram. This will cause erroneous judgment when searching the best-fit solution. Thus, the VR is only used as a reference and has not been considered to evaluate the inversion result in the RMT system.

2.4 Virtual source grid and station settings

The RMT monitors earthquake activity in Taiwan, which covers the region from 119.3°E to 123°E, from 21.0°N to 26.0°N and in depth from 6 to 136 km. A 3-D distributed grid is set in this monitoring area with grid size of 0.1° × 0.1° in horizontal and 10 km in depth (see Fig. 2). The total number of virtual sources in this 3-D grid system is 21 154. These gridpoints are subdivided into several parts in the 'Parallel RMT' program as discussed in the next section. The distributions of BATS stations used in the RMT are shown in Fig. 2. We use six BATS stations in the RMT system, five stations located in Taiwan Island and one sited on the Penghu Island. From north to south are YHNB, SSLB, PHUB, YULB MASB and TWKB. The broad-band stations used in this study are equipped with STS-2 (PHUB, YHNB), STS-1 (MASB) and Trillium-240 (SSLB, TWKB, YULB) seismometers and Q330HR dataloggers. The lower corner frequencies are 8.33 mHz (120 s), 4.17 mHz (240 s) and 2.78 mHz (360 s) for STS-2, Trillium-240 and STS-1, respectively. All of these stations provide good data quality and high signal-to-noise (S/N) ratio of real-time continuous broad-band recordings. However, because PHUB and TWKB are sited close to the coastal area, the background noise, which is mainly caused by large sea waves and tides, could contaminate the seismic signal. Thus, a smaller waveform weighting (0.5) is given for the horizontal components (E and N) of these two stations in the moment tensor inversion procedure. The seismograms recorded by other stations are given a full weighting (1.0) in all three components.

Each gridpoint to station pair has six 1-D Green's functions corresponding to six moment tensor elements. The 1-D Green's function is calculated using the frequency–wavenumber (fk) method of Zhu & Rivera (2001) based on a 1-D Taiwan average velocity model proposed by CWB (Table 1; Chen & Shin 1998). A Green's functions database is stored in the hard disk. This database is read only once from hard disk when the 'Parallel RMT' program starts to work. Then all the Green's functions are stored and taken from the memory when performing the moment tensor inversion. By doing so, the time used to read the Green's functions on each virtual source during grid search will be greatly reduced.

Table 1. 1-D velocity model used for Green's functions.

Thickness (km)	V_p (km s^{-1})	V_s (km s^{-1})	Density (kg m^{-3})	Q_p	Q_s
2.0	3.50	1.97	2200	600	300
2.0	4.44	2.57	2400	600	300
5.0	5.25	3.03	2600	600	300
4.0	6.05	3.46	2600	600	300
4.0	6.36	3.66	2700	600	300
8.0	6.66	3.85	2700	600	300
5.0	7.14	4.10	2700	600	300
5.0	7.43	4.27	2800	600	300
15.0	7.71	4.41	2800	600	300
20.0	7.96	4.63	3000	600	300
20.0	8.10	4.63	3100	600	300
200.0	8.23	4.73	3300	600	300

2.5 Parallel RMT

An important aspect of the RMT system is the combination of the moment tensor inversion with grid search through a 3-D virtual source grid to evaluate the best-fit solution in the monitoring area. With this approach, not only the CMT solution but also the event occurrence time, location and magnitude can be obtained simultaneously. It is expected that using more virtual gridpoints can help to increase the resolution of hypocentral locations and enlarge the monitoring area. However, an increase in the number of virtual source points would lead to a large expansion of grid search time, making the evaluation of a best-fit solution difficult to perform in real time. To resolve this problem, we develop a parallel real-time moment tensor inversion program ('Parallel RMT'), which essentially divides the 3-D gridpoints into present computing nodes; each node deals with only the divided part of 3-D grid, and thus increases the number of total virtual source points and promotes program performance. Message Passing Interface (MPI, Gropp *et al*. 1996) is applied as the communicant between the computing nodes in the parallel computing process. Using the 'Parallel RMT' program within a 32 CPU cores cluster, the RMT system can complete one grid search throughout the monitoring area of every 2 s in real time.

2.6 Event detecting

The example of an earthquake successfully detected by the RMT system is shown in Fig. 3. A continuous real-time monitoring result for Taiwan can be seen in the link: http://rmt.earth.sinica.edu.tw/rmt_demo.htm. An earthquake is detected when: (1) the MR is larger than the threshold (MR = 60), and (2) a peak MR appears (at t seconds) that is no larger than the MR found previously and after 20 s ($t \pm 20$ s).

3 RMT MONITORING RESULTS

The RMT system has been utilized online for more than 1 yr since 2012 January to present. Offline RMT analysis was also carried out for events listed in the CWB earthquake catalogue from 2010 to 2011. All the earthquake parameters for magnitude ≥4 determined by RMT are shown in Table 2. The total number of detected earthquakes is 302; their epicentres and focal mechanisms are shown in Fig. 4. About 60 per cent of these events are located offshore east of Taiwan. The smallest magnitude is M_w 2.8 and only two events are larger than M_L 6 (as retrieved from the CWB earthquake catalogue) occurred during this time period. These two events are the 2010 Jiashian earthquake (M_L 6.4; No. 7 in Table 2) and 2012 Wutai earthquake (M_L 6.4; No. 93 in Table 2). Both of these two events are located in southern Taiwan.

In order to evaluate the system performance of RMT, we compare the source parameters (event time, location and magnitude) taken from CWB earthquake catalogue with those determined by RMT. Fig. 5 shows the difference of RMT and CWB source parameters in location. In the horizontal component (see Figs 5a, b and d), the

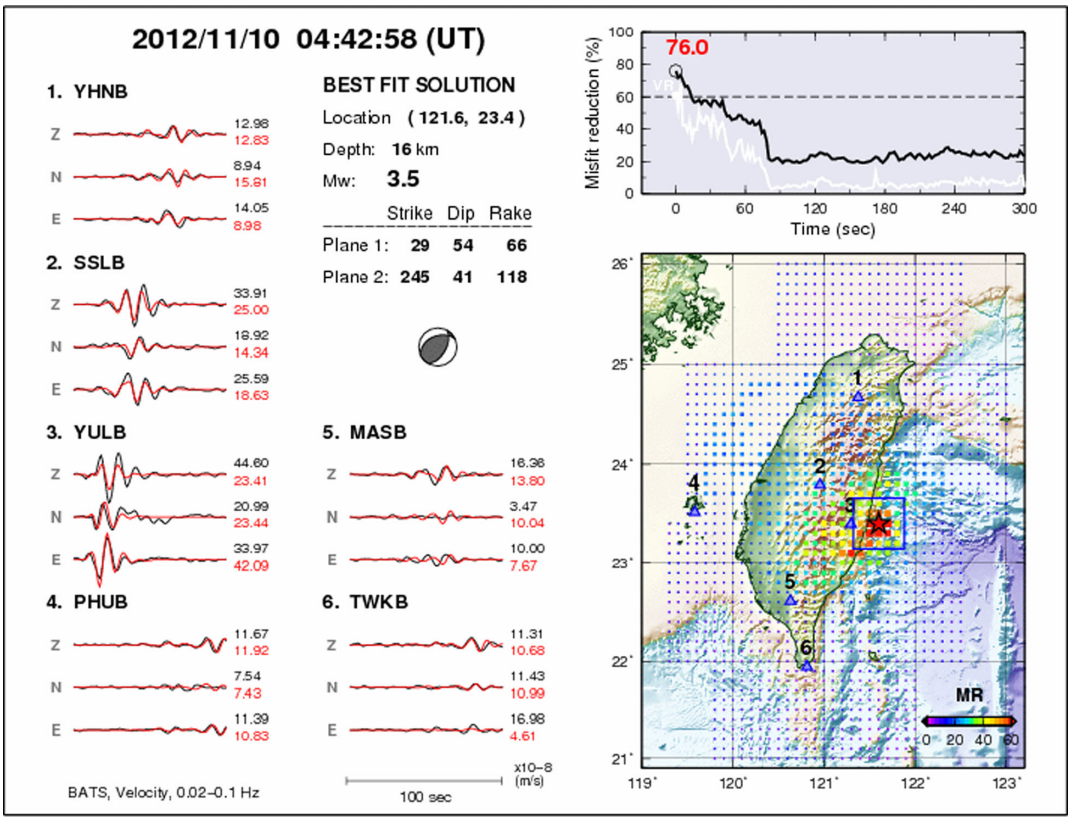

Figure 3. Example of an earthquake successfully detected by the RMT system (the continuous real-time monitoring result can be seen in the link: http://rmt.earth.sinica.edu.tw/rmt_demo.htm). The left panel shows the comparison between the real-time BATS data (black lines) and the synthetic waveforms (red lines). The maximum ground velocity is shown at the end of each waveform. The continuous misfit reduction (MR) of the best-fit solution is presented in the upper right panel. The variance reduction (VR) is also presented in the background and shown as a thin white line. The lower right panel shows the surface projection of the largest MR values in all depths in the monitoring area (MR map). The epicentre of the detected event is shown by a red solid star and highlighted with a blue open square in the MR map.

differences are mostly between $\pm 0.1^\circ$ with the mean value close to 0.0° in both longitude and latitude. For the vertical component (or hypocentral depth), the major differences are between 0 and 10 km, with similar percentage in 0 and +10 km (Fig. 5c). Since the resolution of the RMT in horizontal and vertical are 0.1° and 10 km, respectively (the interval of virtual source grid), the results of the hypocentral location determined by RMT are comparable to the CWB earthquake catalogue. The difference in the event occurrence time between CWB and RMT reports is usually between ± 2 s (see Fig. 6). Again, this falls into the temporal resolution of RMT system, which updates the monitoring result every 2 s.

Fig. 7 shows the comparison between the M_w determined by RMT, M_L obtained from CWB earthquake catalogue and M_w taken from BATS CMT reports. Clear linear relationships can be observed between M_w(RMT) versus M_L(CWB) and M_w(RMT) versus M_w(BATS; see Fig. 7a). Usually, the CWB M_L has larger magnitude compared to the M_w taken from RMT. The maximum difference in magnitude between the two catalogues is -1.0; the averaged differences and standard deviations are -0.45 ± 0.21 (Fig. 7b). This description becomes slightly larger when the magnitude increased. Conversely, the BATS M_w usually has a smaller magnitude compared to M_w taken from RMT. However, the difference is not so obvious. It is less than 0.3 magnitude unit on average. Again, the description becomes slightly larger when the magnitude increased. In all, the moment magnitude M_w determined by RMT is usually between the local magnitude M_L taken from CWB earthquake catalogue and the moment magnitude M_w from BATS CMT reports.

The RMT system analyses the six moment tensor elements in a full inversion; the isotropic and compensated linear vector dipoles (CLVDs) components are then removed to determine the focal mechanism (strike, dip and rake) of the event. In order to evaluate the quality of focal mechanism determined by RMT, we use the Kagan angle (Kagan 1991) to see the difference of focal mechanism (only double-couple part) between BATS CMT and RMT. The Kagan angle is a measure of the difference between the orientations of two seismic moment tensors. Kubo *et al*. (2002) indicates that two focal mechanisms are similar when the Kagan angle is less than 30°. On contrary, a Kagan angle of 120° means that the focal mechanisms are significantly different. The result of Kagan angle from the comparison between BATS CMT and RMT is shown in Fig. 8. Most of the rotated angles are smaller than 50° (with about 63 per cent $< 30^\circ$ and 72 per cent $< 40^\circ$), which indicates that the focal mechanism determined from BATS CMT and RMT are very close.

Note that the azimuthal coverage of events located offshore on the north or south of the Taiwan Island is poor because most of the BATS stations are located on the island. Fortunately, there are few earthquakes occurred in these areas. During our analysis time period (from 2010 to 2012), no earthquake had been detected offshore on northern Taiwan and only one earthquake occurred in southern offshore. The same azimuthal coverage problem also happened on BATS CMT since BATS use the same broad-band station array, which is mostly located on the island. Thus, the difference of Kagan angles between BATS CMT and RMT is not referred to the station azimuthal coverage.

Table 2. Event list for the earthquake determined by the RMT with magnitude $M_w \geq 4.0$.

No.	Date (yyyy/mm/dd)	Time (hh:min:ss)	Time shift (s)	Long. (°E)	Lat. (°N)	Depth (km)	Strike (°)	Dip (°)	Rake (°)	M_w	MR (per cent)
1	2010/01/01	17:34:46	0	121.6	23.8	36	5	63	80	4.4	82.3
2	2010/01/04	19:27:37	+1	121.8	24.2	46	214	79	162	4.7	86.8
3	2010/01/13	10:14:48	−3	121.6	24.0	26	53	28	91	4.0	75.2
4	2010/01/19	06:09:27	+1	121.6	23.8	36	346	76	45	4.7	78.3
5	2010/02/22	05:21:05	−7	123.0	24.0	26	241	59	59	5.1	72.0
6	2010/02/26	01:07:58	−2	122.9	23.6	46	43	74	154	5.3	54.4
7	2010/03/04	00:18:54	+4	120.7	23.1	26	162	77	74	6.1	77.0
8	2010/03/04	07:07:14	+2	122.1	23.1	16	35	88	147	4.2	68.0
9	2010/03/04	08:08:00	0	120.7	23.1	16	177	89	84	3.8	63.0
10	2010/03/04	08:16:16	+2	120.7	23.1	16	170	87	79	4.8	67.1
11	2010/03/08	09:26:23	−7	120.4	23.3	16	339	89	−60	4.3	71.9
12	2010/03/09	05:52:20	−2	121.0	24.0	16	348	70	6	4.0	70.4
13	2010/03/18	09:01:36	−1	122.0	24.4	36	145	34	60	4.2	67.5
14	2010/03/18	16:54:00	−1	122.0	24.4	36	138	32	50	4.1	68.9
15	2010/03/26	23:07:54	0	121.7	24.1	56	235	82	−32	4.4	85.2
16	2010/04/09	11:49:54	0	122.0	24.8	106	126	59	127	4.3	72.8
17	2010/04/11	04:57:31	−3	122.1	23.2	26	2	68	55	4.9	69.0
18	2010/04/13	14:29:29	−3	121.3	23.1	16	186	72	−31	4.5	75.6
19	2010/04/13	20:49:08	−2	121.3	23.1	16	188	78	−29	4.7	75.2
20	2010/04/23	01:49:48	−1	122.4	24.6	86	70	33	135	4.3	67.2
21	2010/05/02	18:00:14	+1	120.6	23.0	16	351	89	−85	4.3	70.0
22	2010/06/14	17:17:46	0	121.6	24.1	26	30	76	91	4.4	77.9
23	2010/06/15	00:31:18	+1	121.6	24.1	26	33	73	95	5.3	77.2
24	2010/06/18	01:08:44	0	121.7	24.2	16	163	15	−13	4.4	72.0
25	2010/06/25	04:28:05	−1	122.1	24.5	56	219	61	146	3.9	71.5
26	2010/06/26	18:05:52	−3	121.6	24.8	76	9	61	163	4.6	84.8
27	2010/07/02	19:11:32	+4	120.8	23.0	16	238	10	−19	4.3	62.1
28	2010/07/08	19:43:38	0	122.0	24.4	26	152	70	−74	4.9	70.8
29	2010/07/09	00:41:20	+2	122.6	24.6	96	215	39	17	4.9	63.7
30	2010/07/17	09:04:17	+1	121.6	23.5	46	30	66	73	4.5	72.5
31	2010/07/18	13:03:25	−3	122.6	24.0	36	295	16	136	5.0	63.6
32	2010/07/25	03:52:10	−1	120.7	22.9	26	198	7	0	5.0	76.9
33	2010/07/31	14:49:06	+1	120.6	23.0	16	171	74	81	4.2	71.9
34	2010/08/30	08:45:09	−2	120.9	25.5	6	21	81	−60	4.7	73.9
35	2010/09/11	22:41:07	+2	121.7	24.4	46	30	88	117	4.1	82.0
36	2010/09/15	08:47:23	−1	121.4	23.2	16	7	60	47	4.1	80.7
37	2010/09/19	05:24:04	0	122.0	24.4	36	113	39	−5	4.1	57.8
38	2010/09/20	03:17:08	0	121.6	23.7	36	3	66	60	4.5	66.3
39	2010/09/28	13:10:13	0	121.6	24.1	26	45	68	58	4.2	78.3
40	2010/09/28	17:33:53	−8	121.8	24.1	16	233	30	−64	4.5	73.5
41	2010/09/30	19:56:00	0	121.9	24.9	86	216	47	44	4.1	67.1
42	2010/10/02	19:23:12	0	121.7	24.4	26	78	64	−25	4.5	68.7
43	2010/11/08	13:01:21	0	120.4	23.3	16	303	42	53	4.5	73.8
44	2010/11/12	13:08:50	−4	122.7	24.1	36	59	72	80	5.1	69.3
45	2010/11/12	15:39:01	0	120.5	22.2	36	209	58	−21	4.8	73.0
46	2010/11/16	03:00:35	−1	121.7	24.1	26	26	63	66	4.1	70.8
47	2010/11/21	12:31:46	+1	121.6	23.9	46	13	81	67	5.5	77.3
48	2010/11/26	15:13:45	+1	121.7	24.2	26	30	80	68	4.5	79.0
49	2010/12/06	02:14:12	−1	121.4	23.7	16	134	20	76	4.3	70.9
50	2010/12/07	02:46:15	0	121.4	23.0	36	136	78	−30	4.4	79.8
51	2011/01/31	20:53:16	+1	121.7	24.2	26	195	88	−68	4.5	78.2
52	2011/02/01	08:16:32	−6	121.8	24.2	16	260	21	−16	5.0	77.7
53	2011/02/05	12:46:32	−3	122.2	24.6	66	66	16	120	4.0	69.0
54	2011/02/07	05:55:02	−2	121.7	24.1	26	77	51	124	4.3	75.0
55	2011/03/16	13:12:17	−1	120.7	22.6	36	222	33	−62	4.2	82.6
56	2011/03/18	11:12:24	+1	121.7	24.2	16	220	77	−80	4.0	72.7
57	2011/03/20	08:00:51	−5	121.7	22.4	16	211	68	119	5.0	64.4
58	2011/03/26	07:19:12	−2	121.9	25.0	96	112	81	71	4.1	54.1
59	2011/03/30	04:22:32	−2	121.5	23.9	16	72	35	112	4.2	73.5
60	2011/05/03	15:52:34	−2	121.8	23.9	46	86	21	162	4.7	76.9
61	2011/05/06	21:31:51	−3	121.5	23.2	26	346	49	42	4.4	81.1
62	2011/05/22	01:34:12	−1	121.8	24.2	16	206	58	−34	4.9	61.2
63	2011/05/22	21:07:16	−2	121.1	23.9	26	30	36	97	4.3	87.5
64	2011/05/24	18:32:05	0	121.5	23.4	36	169	86	−37	4.0	73.9
65	2011/06/10	01:25:22	−1	121.6	23.6	36	351	61	55	4.6	77.2

Table 2 (*Continued*.)

No.	Date (yyyy/mm/dd)	Time (hh:min:ss)	Time shift (s)	Long. (°E)	Lat. (°N)	Depth (km)	Strike (°)	Dip (°)	Rake (°)	M_w	MR (per cent)
66	2011/06/19	10:18:55	−1	121.9	24.7	76	55	51	128	4.4	86.5
67	2011/06/26	00:31:22	+1	122.0	24.3	36	21	72	120	4.2	73.6
68	2011/07/03	12:30:44	−5	122.1	24.8	76	70	35	152	4.3	83.2
69	2011/07/06	05:22:58	+2	121.7	24.3	26	44	72	88	4.3	82.7
70	2011/07/06	11:59:00	0	121.8	24.3	26	50	61	114	4.4	82.0
71	2011/07/07	15:52:20	+1	121.7	24.3	26	43	73	99	4.2	78.9
72	2011/07/12	11:17:11	+1	121.5	23.5	26	18	49	100	4.7	82.7
73	2011/07/17	18:45:24	−1	121.6	23.8	26	358	68	65	4.2	76.0
74	2011/07/19	14:01:10	−2	121.6	24.0	26	74	42	128	4.3	76.7
75	2011/08/10	19:25:55	0	121.7	23.4	26	236	50	134	4.1	82.3
76	2011/08/11	22:07:33	−1	121.6	23.8	36	355	73	58	4.3	80.4
77	2011/08/25	09:35:14	−1	121.9	23.1	16	5	25	46	4.1	72.2
78	2011/08/31	11:22:32	+9	120.8	21.9	16	150	41	62	4.3	74.2
79	2011/09/09	03:26:59	+1	120.9	22.3	16	175	72	18	4.4	69.8
80	2011/09/09	05:52:12	+1	120.9	22.3	16	79	69	164	4.0	66.9
81	2011/09/21	22:18:33	0	121.7	24.1	26	38	59	72	4.6	81.5
82	2011/09/22	01:00:59	0	121.6	23.8	36	3	67	70	4.3	81.0
83	2011/10/09	15:54:26	−2	121.0	22.5	26	103	51	132	4.3	73.8
84	2011/10/31	15:17:04	0	122.0	24.9	76	119	76	110	4.1	63.1
85	2011/12/02	00:55:24	0	121.3	23.0	16	28	46	65	4.4	76.4
86	2011/12/04	10:13:04	−1	122.1	24.7	66	76	46	149	4.3	78.7
87	2011/12/15	00:35:42	−1	121.8	23.7	36	231	64	117	4.3	72.5
88	2012/01/04	06:59:57	−9	121.7	23.9	16	275	31	−17	4.1	62.9
89	2012/01/21	00:50:02	−4	122.5	24.2	26	53	71	99	4.4	66.9
90	2012/02/04	02:54:23	+1	122.7	24.7	96	213	75	−12	4.7	61.5
91	2012/02/05	16:25:11	+1	121.0	22.5	26	138	41	−29	4.5	67.8
92	2012/02/06	03:48:28	0	121.0	22.4	26	36	87	93	4.2	72.4
93	2012/02/26	02:35:00	+1	120.7	22.7	36	179	49	87	5.8	78.9
94	2012/03/04	17:52:15	0	122.7	24.1	46	115	50	3	4.4	69.8
95	2012/03/21	23:44:38	−1	121.6	23.2	46	235	61	128	4.4	74.5
96	2012/04/07	19:59:18	−1	121.7	24.1	26	357	66	47	4.2	78.6
97	2012/04/12	10:39:25	0	120.4	23.4	16	15	32	70	4.0	64.0
98	2012/04/19	01:58:09	−1	121.7	24.1	26	11	77	56	4.9	81.5
99	2012/04/27	14:48:36	−1	121.8	23.8	36	42	36	85	4.2	72.5
100	2012/04/27	21:08:18	0	120.7	22.7	26	167	67	87	3.9	88.0
101	2012/05/30	07:25:42	−2	121.0	23.2	16	259	89	179	4.2	75.5
102	2012/06/05	09:56:30	−3	122.4	24.3	36	277	18	133	4.7	65.0
103	2012/06/06	01:08:35	+9	121.5	22.6	26	180	36	−69	5.6	66.9
104	2012/06/09	21:00:18	+5	122.1	24.4	66	191	57	52	5.8	67.4
105	2012/06/09	21:54:21	+1	122.2	24.5	66	176	68	47	4.3	65.4
106	2012/06/10	06:23:29	−1	121.7	23.9	36	355	71	69	4.2	80.3
107	2012/06/13	08:22:20	+1	121.3	24.7	6	14	52	−20	4.2	89.5
108	2012/06/14	16:15:13	+1	121.5	23.7	6	1	65	63	4.8	68.2
109	2012/06/14	19:30:56	0	121.5	23.7	16	33	89	51	4.5	78.5
110	2012/07/04	20:05:47	−4	121.0	21.5	26	45	72	110	4.5	66.5
111	2012/08/14	10:55:43	0	121.5	24.1	26	87	61	143	4.4	77.1
112	2012/08/16	17:41:00	0	121.5	24.1	26	89	54	152	4.0	74.0
113	2012/08/31	12:11:40	0	120.9	24.7	6	94	56	168	4.0	80.7
114	2012/09/04	20:00:18	+2	121.0	22.2	26	63	83	121	5.1	68.6
115	2012/09/05	03:45:30	−4	122.6	24.0	36	65	74	83	4.5	65.0
116	2012/09/24	21:57:33	+2	121.2	22.9	16	59	32	62	4.1	78.0
117	2012/10/13	08:27:51	−1	121.5	24.1	26	6	36	81	3.8	66.9
118	2012/10/20	08:49:39	0	122.5	24.4	76	192	79	84	4.3	63.5
119	2012/10/25	10:31:18	0	120.4	22.5	36	15	49	−75	5.0	72.6
120	2012/11/05	13:40:30	−2	121.5	23.8	16	95	59	148	4.2	79.8
121	2012/11/20	17:09:02	−6	121.7	22.4	16	6	27	68	4.8	64.8
122	2012/11/21	22:25:26	−3	122.5	24.0	26	279	17	118	4.6	64.9
123	2012/11/29	03:12:53	+2	121.3	22.7	76	140	76	106	4.3	78.7
124	2012/12/02	17:45:37	0	121.5	24.0	16	71	66	139	4.6	69.4
125	2012/12/02	19:43:31	−2	121.6	23.9	16	37	29	81	4.3	72.6
126	2012/12/11	10:32:04	+1	121.6	24.1	26	19	84	39	4.2	73.4
127	2012/12/24	03:17:52	+1	121.3	22.5	66	217	19	−6	4.4	62.1
128	2012/12/26	02:06:38	−3	122.6	23.9	36	65	80	79	4.6	62.2
129	2012/12/30	16:03:26	−1	120.9	23.5	6	338	79	−9	4.6	75.5

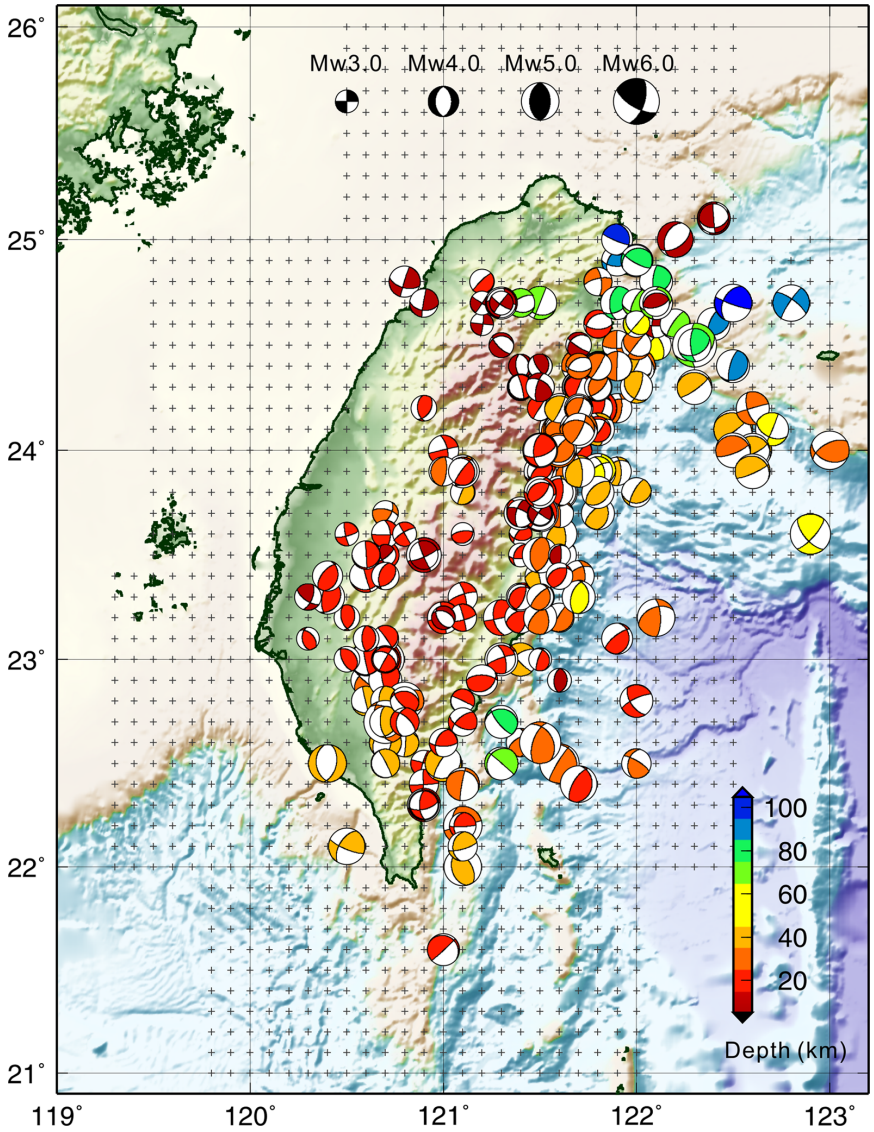

Figure 4. The RMT analysis results. A total number of 302 earthquakes determined from RMT online monitoring (2012) and offline analysis (2010–2011) is shown. Beach balls are their focal mechanisms; different hypocentral depths are presented with varied colours.

4 DISCUSSION

4.1 Time and location

It is worth noting that the earthquake location and focal mechanism determined by RMT can be different from CWB earthquake catalogue and BATS CMT reports. Because the RMT determined the centroid based on the best-fit location of full waveform moment tensor inversion results while the CWB report is determined based on the traveltime of first arrivals, which is sensitive to revealing the initial rupture point. The initial rupture and the centroid might have a shift in both time and space, especially for large earthquakes. Furthermore, the system biases of two methods could also cause differences of event time and location. These differences will further influence the inversion result of seismic moment tensor. We find in some specific cases that the event time, location and focal mechanism of northeast offshore earthquakes can sometimes have an obvious difference with respect to that reported in the CWB catalogue and BATS CMT solutions (see Fig. 9). To evaluate the robustness of RMT, we perform forward 3-D wave propagation simulations for these specific events and compare the synthetic waveforms determined from the source parameters provided by RMT and BATS CMT solutions. The simulations are based upon spectral-element method with a fully 3-D tomography model (Lee *et al*. 2013). Results show that the synthetics determined from RMT fit the observed waveforms better in both timing and amplitude compared to the BATS CMT solutions. This could be due to the differences in event time and location taken from CWB earthquake report that further influence the CMT inversion result of BATS.

Reliable determination of source parameters for offshore earthquakes east of Taiwan is an important seismological task because more than 60 per cent of the earthquakes in Taiwan occur in this area. Since the moment tensor inversion is based on the concept of earthquake centroid, the RMT utilizes the best-fit gridpoint (the centroid location) to determine the moment tensor and focal mechanism that could be more reliable, especially for large earthquakes because their nucleation and centroid locations are usually different. Once there are more inland and offshore events determined by RMT, a comprehensive analysis of seismic moment tensors and their implications to Taiwan tectonic setting will be addressed in detail.

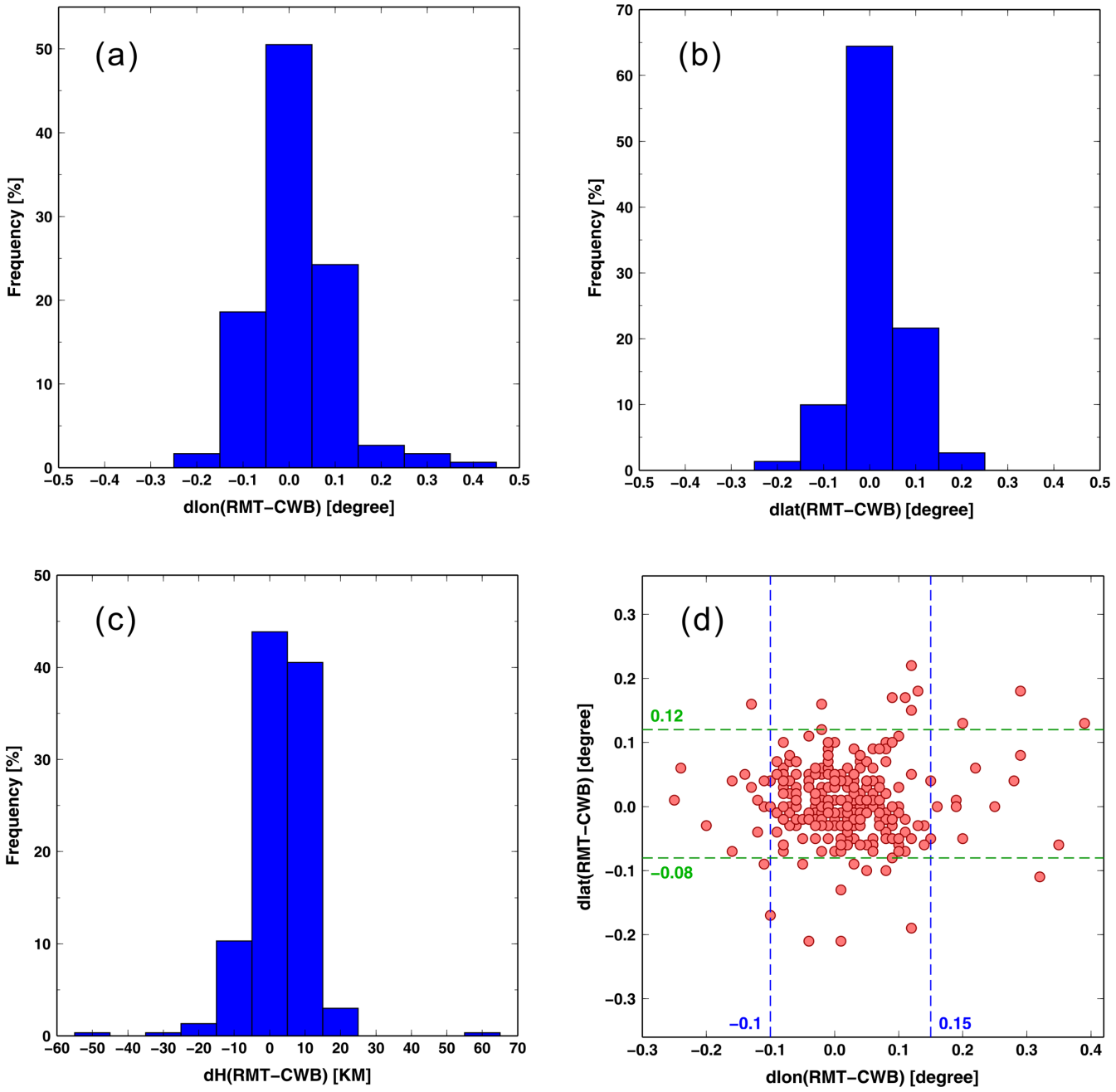

Figure 5. Comparison of source parameters between RMT analysis results and CWB earthquake catalogue: (a) histogram of the difference in longitude, (b) histogram of the difference in latitude, (c) histogram of the difference in hypocentral depth and (d) difference pairs in horizontal (longitude and latitude).

4.2 Station redundancy

Because the moment tensor inversion analysis utilizes full waveforms from all three components, it can be done with only a few stations (Dreger & Helmberger 1993). For example, the GRiD MT system in Japan uses three inland stations (per grid) to monitor earthquakes offshore, east of the Tohoku area. However, when a missing data problem occurs, the GRiD MT is unable to accurately detect an earthquake with just one station (Tsuruoka *et al*. 2009a). Unlike the GRiD MT, the RMT system uses six BATS stations in Taiwan. When one or two stations have missing data problems, the remaining stations can still provide good azimuth coverage. The traveltime and radiation information can be retrieved from other stations with full waveforms in all three components. This implies that the use of six BATS stations itself can be regarded as a redundant seismic network in the RMT system. For example, the SSLB station was down during the 2012 December 11 earthquake (M_w 4.2). It still worked well to find the correct source parameters using the remaining five stations (see Fig. 10). In this case, the system was inverting flat seismograms for the missing data.

4.3 Teleseismic events

The RMT system monitors earthquake activity by using long-period waveform between 10 and 50 s. This period could be overlapping with teleseismic events which are dominated by long-period waveforms, and thus result in an erroneous judgment as a local event in

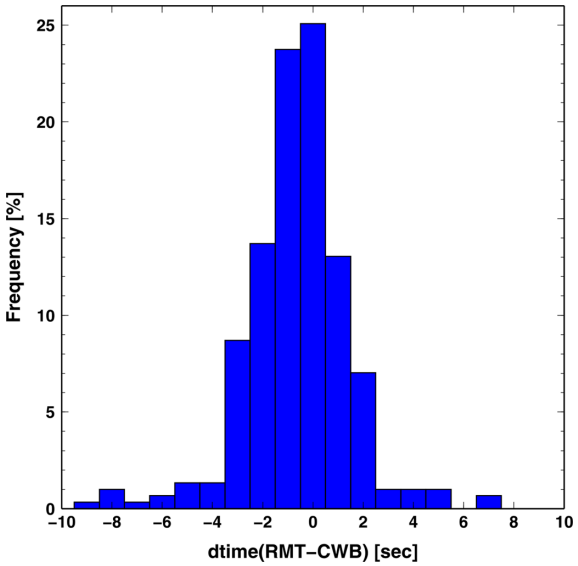

Figure 6. Histogram of the difference in event time between RMT analysis results and CWB earthquake catalogue.

the RMT. However, after online monitoring for more than 1 yr, we find that the RMT system can deal with this problem well. This is because the first teleseismic arrival reaches the local seismic network at almost the same time that none of the Green's functions in all virtual source points can explain the observed arrival time pattern. Furthermore, even though the later phases of a teleseismic event usually have large amplitudes, their phases and arrival times at each station are incoherent (similar to the low-frequency random noise) that cannot be explained by Green's functions. Thus, the teleseismic waveform cannot increase the value of MR (always <60) to result in false detection. An example of the response of the RMT system during 2012 April 11 off the west coast of northern Sumatra event (M_w 8.6) is shown in Fig. 11.

For an event that occurs in a regional distance like in Japan, the maximum MR is usually less than 60. Only a few cases show MR between 60 and 65. The increase of MR (>60) of the regional earthquakes is due to the first arrival (*P* wave). Unlike the teleseismic event that the first arrival reaches BATS stations at almost the same time, the regional event may have an arrival recorded by one station earlier. In this case, the inversion will try to fit this specific phase with local Green's functions and sometimes the MR can increase significantly due to a good fitting on that specific waveform. This kind of false detection can be easily eliminated by increasing the MR threshold (MR = 65) or adding another constraint in the system, that is, considering the individual waveform misfit on each seismogram. In addition, the *W*-phase can provide very good information for the point source moment tensor inversion (Kanamori & Rivera 2008; Hayes *et al*. 2009). The *W*-phase has incorporated into GRiD MT system in Japan to obtain the MT in real time (Tsuruoka *et al*. 2009b). Similar use of the *W*-phase to monitor regional events close to Taiwan (i.e. in the Ryukyu and Manila trenches) will be considered in the RMT system in future.

4.4 Monitoring performance

Using high-quality broad-band data from BATS, small earthquakes ($M < 4$) can also be detected by RMT. Fig. 12 shows the relationship between moment magnitude (M_w) and MR of the events determined by RMT. It shows that smaller earthquakes usually have a lower MR,

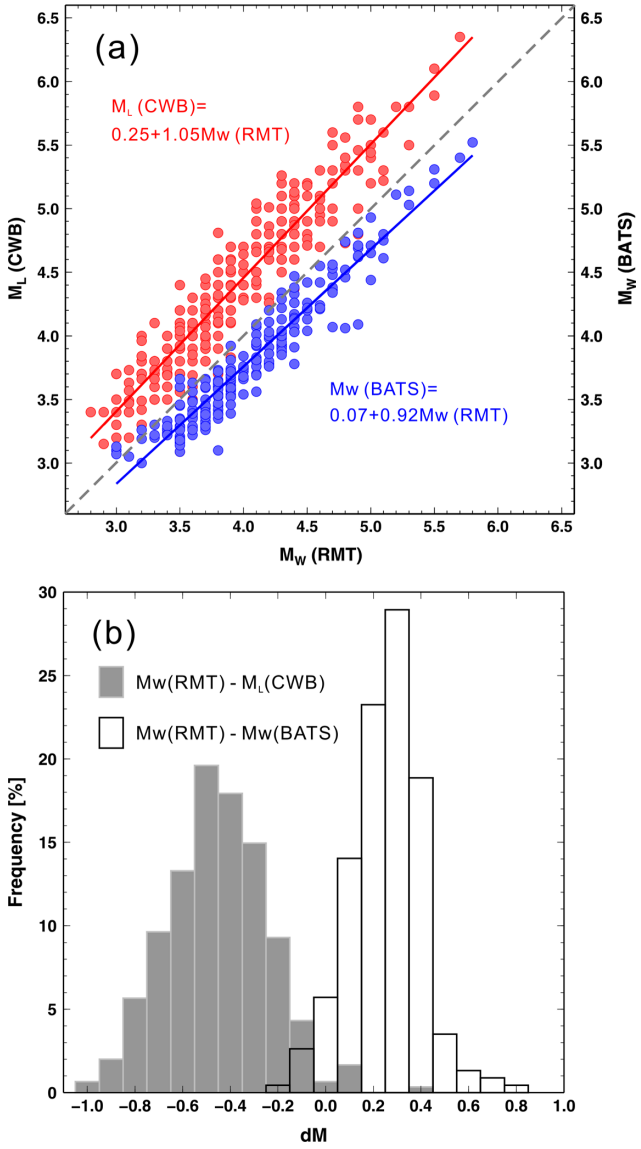

Figure 7. Comparison between the moment magnitude of RMT, local magnitude of CWB and moment magnitude of BATS CMT catalogues: (a) Correlation of the magnitudes determined from different catalogues. Red solid circles show the magnitude correlation of M_w (RMT) and M_L (CWB). Blue solid circles are the magnitude correlation of M_w (RMT) and M_w (BATS). (b) Histogram of the differences in magnitude determined from RMT, CWB and BATS catalogues.

especially when M_w is lower than 3.7. When considering a threshold of MR = 60 to evaluate the occurrence of an earthquake in the region, we find that 82.7 per cent of the total events can be detected, including 19.5 per cent of the events that have M_w lower than 3.7. If we target only $M_w \geq 3.7$ earthquakes, 93.2 per cent events can be caught by the RMT system. The missed 6.8 per cent of the 3.7+ earthquakes are mainly caused by: (1) deep events which induce weak shaking at ground surface, (2) low S/N ratio due to noisy data, which are usually resulted from bad weather condition, such as torrential rain or typhoon, especially for the stations close to the coastal area and (3) the contamination of large teleseismic event. The amplitude of waveform of the local small-to-moderate event is relatively weak, which is embedded in the large surface waves originated from big teleseismic earthquake. It is expected that a smaller MR threshold can help to detect more small earthquakes.

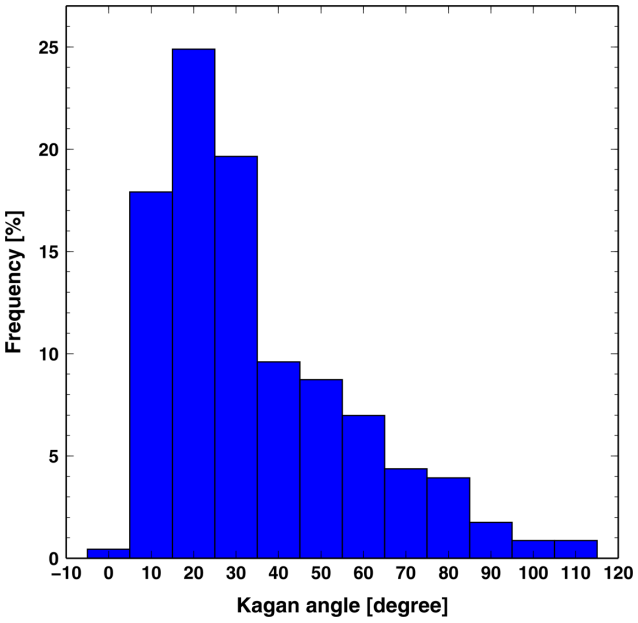

Figure 8. Histogram of the Kagan angle determined from the comparison between BATS CMT and RMT.

However, the number of false detections will be increased due to low S/N ratio of small earthquakes. Since the purpose of RMT focuses on providing the source parameters for moderate-to-large earthquakes ($M \geq 4$), the use of MR = 60 as the threshold is appropriate for monitoring target events.

Nevertheless, there are several false alarms that occurred during the online monitoring time period (from 2012 to present). Most of the false alarms are due to regional events which can be easily eliminated by increasing the MR threshold (MR = 65) or adding another constraint in the system as discussed in the previous section. A few false alarms are due to station problem, such as the regular checking or testing of seismometer. However, some unidentified false alarms are also found which might be caused from the anomalous ground shakings resulted from large landslides (on the land as well as seabed), low-frequency events or others.

Concerning the performance of timing, the recent RMT system provides all point source parameters within 117 s once the earthquake occurs. The waveform time window used is 100 s long, and the system takes 15 s for time synchronization. The times needed in these two parts are fixed and cannot be reduced. It takes another 2 s for data processing, inversions, grid search and plotting the results to show on webpage. Thus, the RMT updates the monitoring information every 2 s and the total system latency is 117 s (or less than 2 min). Our analysis results indicate that 2 s updated rate is good enough to obtain the precise source parameters in the RMT system. Of course, if this time interval can be reduced, such that an update is provided every second or less, the monitoring performance will be improved further. By the use of 32 MPI threads in the 'Parallel RMT' program, the inversion and grid search through all 21 154 virtual sources take less than 0.5 s in one iteration. However, in order to provide the real-time monitoring result on the webpage [plotting the monitoring summary via GMT (Generic Mapping Tools) and then converting into PNG (Portable Network Graphics) format], it needs more than 1 s to accomplish. This part works under one MPI thread depending only on the performance of a single CPU core that cannot be parallelized. According to Moore's law (Moore 1965), the number of transistors on integrated circuits doubles approximately every 2 yr. We can expect that when the single thread computing performance is improved in the next generation CPU, this problem will be resolved straightforwardly.

4.5 Future studies

The recent RMT system utilizes 1-D Green's functions based on a 1-D Taiwan average velocity model (Chen & Shin 1998). In most of the cases, the 1-D Green's functions can work sufficiently well for the low-frequency period between 10 and 50 s in Taiwan. However, we find in some specific cases that the performance of 1-D Green's functions must be evaluated, such as, when an earthquake occurs northeast offshore, which is far away from the island (∼123°E). The location of the earthquake can sometimes have an obvious difference with respect to that reported in the CWB earthquake catalogue. This could be due to the complex wave propagation path effect caused by the Ryukyu subduction zone. In this case, the 1-D velocity model might not be able to explain the complex path effect even in a low-frequency signal. To deal with this problem, we are preparing to use 3-D Green's functions calculated by spectral-element method based on a new 3-D tomography model (H.-H. Huang *et al.*, 2013), which has improved the resolution in area offshore northeast Taiwan. Furthermore, a finer grid (<0.05° in horizontal and <5.0 km in depth) and a hybrid seismic network, including BATS, CWB marine cable observatory and F-net from Japan (YNG station on Okinawa-ken Yaeyama-gun) can help to improve station coverage. With precise 3-D Green's functions, finer grid, more stations for better azimuth coverage, we can expect that the monitoring performance of RMT can be further improved.

For large earthquake ($M > 7.0$), the rupture duration might be longer and the frequency range that is used in RMT will fall in the slope of the displacement spectra of a large event leading to moment magnitude saturation (Guilhem *et al*. 2013). Also the use of broad-band stations might not be feasible during a large earthquake as they are subject to clipping in the strong motions. We design a procedure to deal with this problem in the RMT system. When the strong ground shaking makes the broad-band recording saturated, the system will automatically remove that record by given a zero weighting on the waveform in the inversion. Thus, the clipped waveforms will not influence the estimate of CMT. We are also planning to develop a multichannel RMT for large earthquakes. In that case, a lower frequency band (0.01–0.033 Hz) and a longer waveform time window (>200 s) will be considered based on low-gain strong-motion recordings. In this case, however, the source information will be obtained after 2 min. A multiple-source moment tensor inversion procedure for monitoring the finite-fault rupture characteristics of big earthquakes ($M > 8.0$) is also planned. These two approaches, which are based on the recent RMT system for large events, will be developed and practiced online in the near future.

4.6 Implication in seismic hazard assessment

A routine CWB earthquake report can provide the information of earthquake origin time, location and local magnitude about 2–5 min after the occurrence of an earthquake. If the earthquake has a larger magnitude, the moment tensor inversion will also be performed. Because this analysis is not done automatically, it needs more time to obtain the CMT solution, usually more than 1 hr. For the RMT monitoring system, all the point source parameters, including event time, location, moment magnitude, moment tensor and focal mechanism can be obtained simultaneously within 2 min. Compared to the routine CWB earthquake report, the RMT has a great

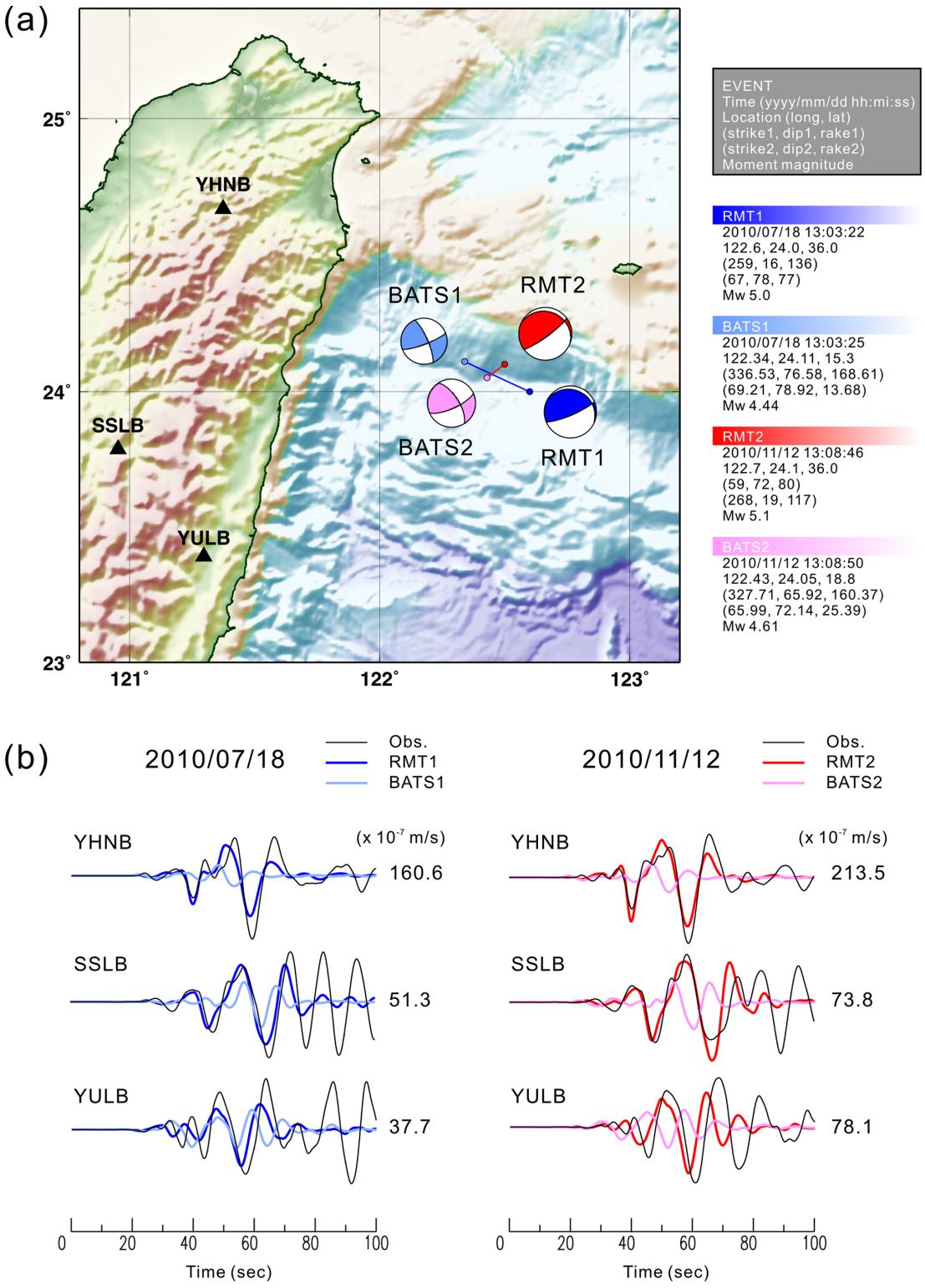

Figure 9. (a) Comparison of specific offshore events between RMT and BATS CMT solutions. Left-hand side shows the map view of their locations and focal mechanisms; right panel lists the detailed source parameters. (b) Comparison between vertical components observed velocity data and synthetic waveforms determined by RMT and BATS CMT solutions. The maximum observed ground velocity is shown at the end of each waveform.

improvement in time saving (see Fig. 13). This is very important for rapid assessment and response to seismic hazards. For example, when a big earthquake occurs along the southernmost Ryukyu subduction zone (Hsu *et al*. 2012), a potential tsunami hazard needs to be taken into account. The tsunami arrives on the east coast in less than 30 min based upon dispersive (DSP) tsunami equations simulation (Saito & Furumura 2009). If all the source information can be obtained within 2 min, especially the focal mechanism, the appropriate government and emergency response agencies can have more time to judge whether people need to evacuate the coastal area

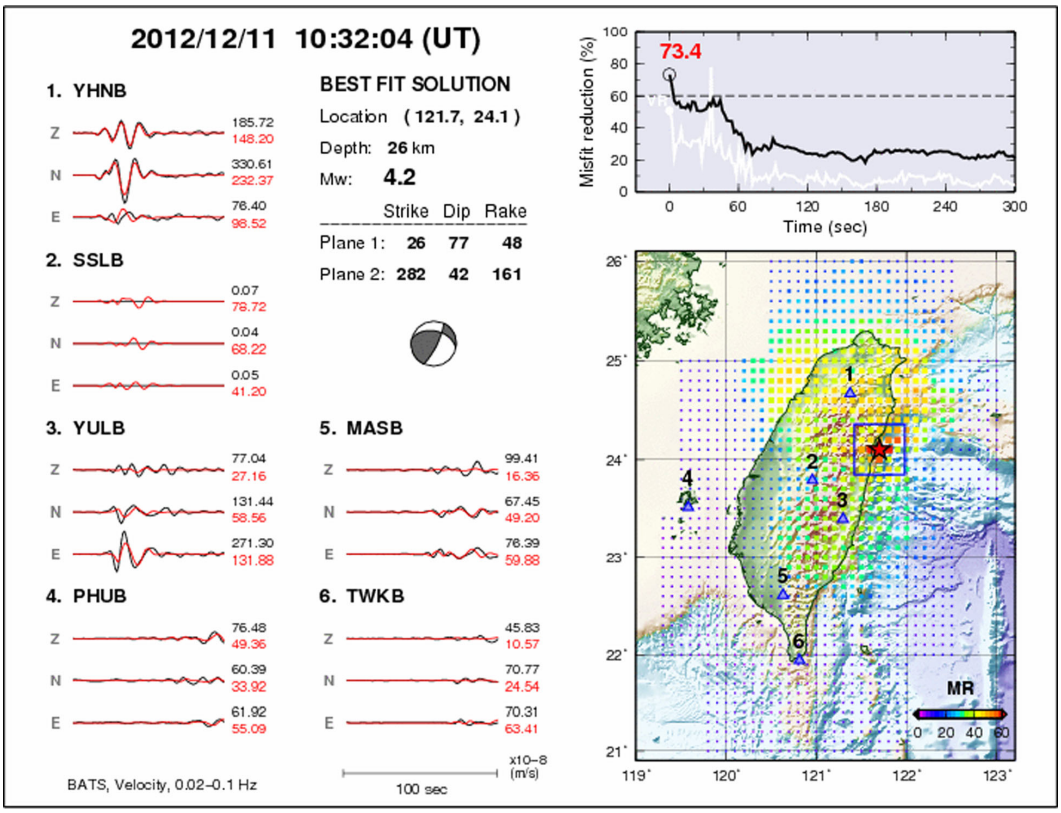

Figure 10. An example of data missing happened in the RMT system. The real-time data of SSLB were missed during the 2012 December 11 earthquake (M_w 4.2). In this case, the system was inverting flat seismograms for the missing data.

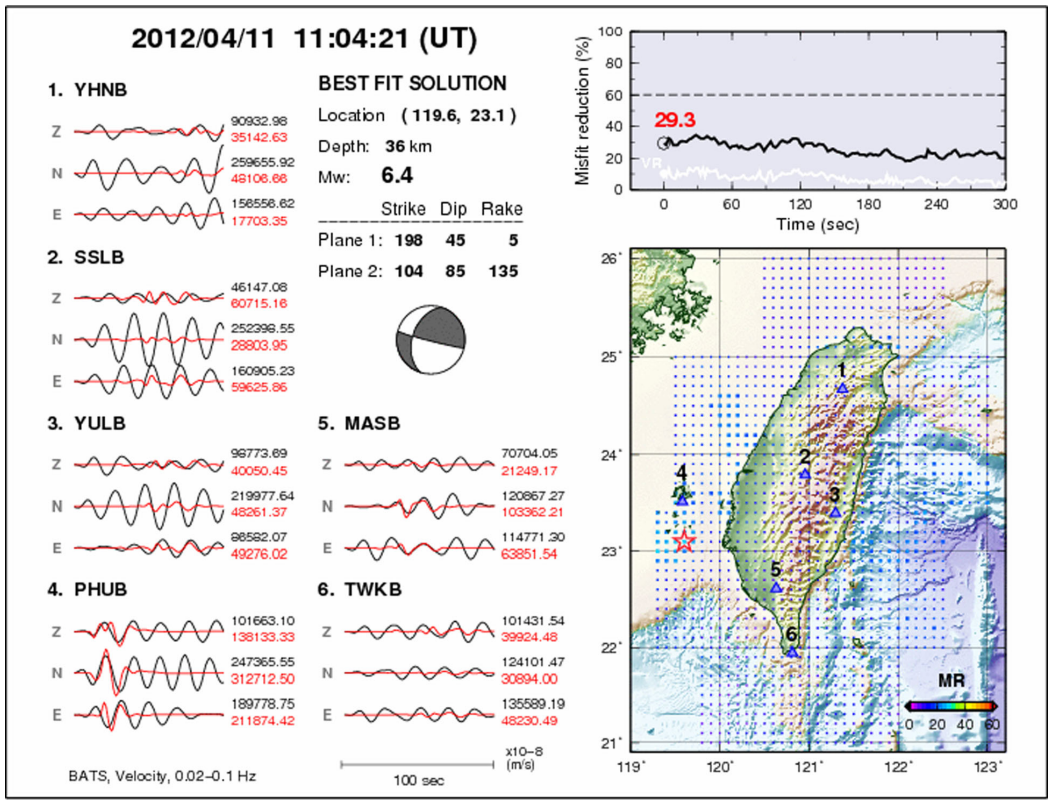

Figure 11. An example of the response of a big teleseismic event in the RMT system. All of the used six BATS stations recorded large long-period surface waves after 2012 April 11 off the west coast of northern Sumatra earthquake (M_w 8.6).

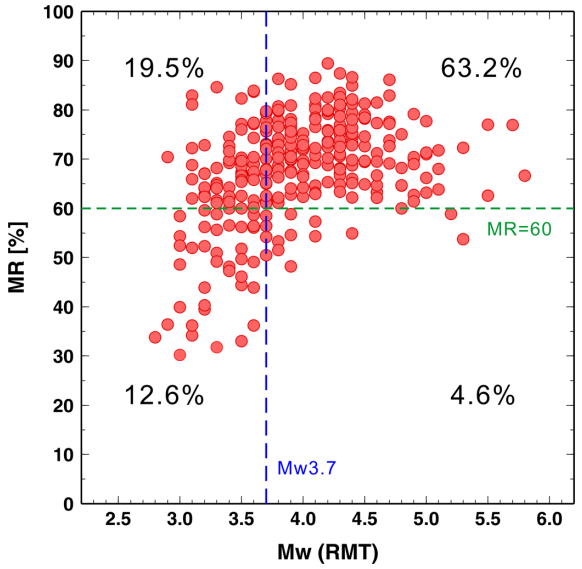

Figure 12. The relationship between moment magnitude (M_w) and misfit reduction (MR) of the events determined by RMT. The green dashed line shows the MR threshold (MR = 60), and the blue dashed line marks the moment magnitude of M_w 3.7. The percentages of the events in each quadrant are also shown.

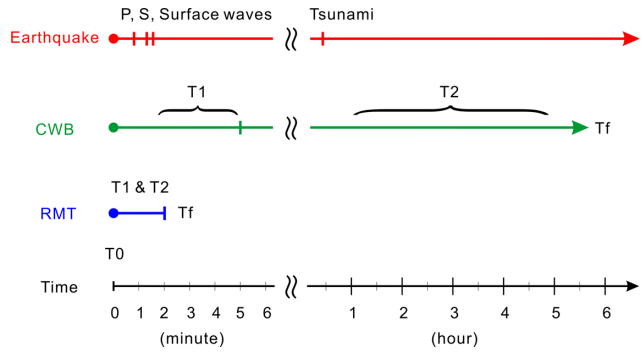

Figure 13. The timelines of the RMT monitoring, CWB earthquake report and the *P* wave, *S* wave, surface wave, as well as tsunami arrivals of a big earthquake occurring offshore northeast of Taiwan. T_0 indicates the event origin time. T_1 is the time to obtain the information of earthquake origin time, location and magnitude; the CMT solution and focal mechanism are determined in T_2. The final earthquake report is obtained at T_f.

or not. In this case, the RMT will play an important role in providing crucial source information in real time.

By connecting the RMT with real-time online earthquake simulation (ROS) system (Lee *et al*. 2013), the real-time earthquake simulation will be achievable. When an earthquake occurs, all the point source parameters, including event time, location, moment magnitude, moment tensor and focal mechanism can be obtained simultaneously within 2 min by RMT. These source parameters will automatically forward to the ROS system to perform an earthquake simulation in 3 min. All the numerical simulation results, including the ShakeMovie and ShakeMap, can be obtained in 5 min after the occurrence of an earthquake. This real-time earthquake simulation result can provide a complete ground shaking information for a rapid response for seismic hazard assessment. Details of the development of ROS and its interaction with RMT will be discussed in another paper (Lee *et al*. 2013).

5 CONCLUSION

We have developed an RMT system to provide the real-time monitoring of the earthquake activity in Taiwan. This system uses BATS continuous broad-band data and searches the best-fitting moment tensor solution from a 3-D distributed virtual source grid. The event origin time, location, magnitude, moment tensor and focal mechanism can be obtained simultaneously within 2 min after an earthquake occurs. We improve the system performance by taking advantage of a parallel computing technique, which basically divided the total virtual sources into several parts depending on the number of computing nodes. This improvement is crucial for the purpose of real-time earthquake monitoring at a regional scale. In addition, the use of six BATS stations can form a redundant virtual seismic network to deal with the data missing problem. The RMT system has been operated online for more than 1 yr (since 2012). The online (2012) and offline (from 2010 to 2011) analyses show that the event origin time, hypocentral location and magnitude determined by RMT are similar to that in the CWB earthquake catalogue. The focal mechanisms are also comparable to solutions in the BATS CMT catalogue.

Our results indicate that the RMT is a robust automatic system that uses long-period wavefield (10–50 s) of broad-band records to monitor the earthquake activities at a regional scale in real time. The real-time source information, especially the focal mechanism, provided by RMT will be crucial in seismic hazard assessment when a big earthquake occurs. Furthermore, all the source parameters provided by RMT will be forwarded to ROS to perform earthquake simulation, which will provide dense ground shaking information in real time. The next stage of the RMT development will include the application of 3-D Green's functions, finer virtual source points and hybrid seismic network to improve both the system performance and station coverage.

ACKNOWLEDGEMENTS

We thank the BATS for providing high-quality real-time broad-band waveform data. We would also like to thank Dr Aurelie Guilhem and one anonymous reviewer for their comment and suggestions, which significantly improved the quality of the paper. This research was supported by the Taiwan Earthquake Research Center (TEC) funded through the National Science Council (NSC) with grant number NSC 100-2628-M-001-007-MY3. The TEC contribution number for this paper is 00095. A part of the research was funded by the ERI's international visiting program.

REFERENCES

Aki, K. & Richards, P.G., 1980. *Quantitative Seismology: Theory and Methods,* 932 pp., Freeman & Co.

Backus, G. & Mulcahy, M., 1976. Moment tensors and other phenomenological descriptions of seismic sources—I. Continuous displacements, *Geophys. J. R. astr. Soc.,* **46,** 341–361.

Bernardi, F., Braunmiller, J., Kradolfer, U. & Giardini, D., 2004. Automatic regional moment tensor inversion in the European-Mediterranean region, *Geophys. J. Int.,* **157**(2), 703–716.

Chen, Y.-L. & Shin, T.-C., 1998. Study of the earthquake location of 3-D velocity structure in Taiwan area, *Meteor. Bull.,* **42,** 135–169.

Dreger, D. & Helmberger, D.V., 1993. Determination of source parameters at regional distances with single station or sparse network data, *J. geophys. Res.,* **98,** 8107–8125.

Duputel, Z., Rivera, L., Kanamori, H., Hayes, G.P., Hirshorn, B. & Weinstein, S., 2011. Real-time W phase inversion during the 2011 off the Pacific coast of Tohoku Earthquake, *Earth Planets Space,* **63**(7), 535–539.

Dziewonski, A.M., Chou, T.-A. & Woodhouse, J.H., 1981. Determination of earthquake source parameters from waveform data for studies of global and regional seismicity, *J. geophys. Res.,* **86,** 2825–2852.

Ekström, G., Nettles, M. & Dziewonski, A.M., 2012. The global CMT project 2004–2010: centroid-moment tensors for 13,017 earthquakes, *Phys. Earth. planet. Inter.,* **200–201,** 1–9.

Fukuyama, E., Ishida, M., Dreger, D.S. & Kawai, H., 1998. Automated seismic moment tensor determination by using on-line broadband seismic waveforms, *Zisin,* **51,** 149–156. [in Japanese with English abstract]

Gropp, W., Lusk, E., Doss, N. & Skjellum, A., 1996. A high-performance, portable implementation of the MPI message passing interface standard, *Parallel Comput.,* **22**(6), 789–828.

Guilhem, A. & Dreger, D.S., 2011. Rapid detection and characterization of large earthquakes using quasi-finite-source Green's functions in continuous moment tensor inversion, *Geophys. Res. Lett.,* **38,** L13318, doi:10.1029/2011GL047550.

Guilhem, A., Dreger, D.S., Tsuruoka, H. & Kawakatsu, H., 2013. Moment tensors for rapid characterization of megathrust earthquakes: the example of the 2011M9 Tohoku-oki, Japan earthquake, *Geophys. J. Int.,* **192**(2), 759–772.

Hanka, W., Heinloo, A. & Jaeckel, K.H., 2000. Networked seismographs: GEOFON real-time data distribution, *ORFEUS Newsl.,* **2**(3).

Hayes, G.P., Rivera, L. & Kanamori, H., 2009. Source inversion of the W phase: real-time implementation and extension to low magnitudes, *Seismol. Res. Let.,* **3,** 800–805.

Hsu, Y.-J., Ando, M., Yu, S.-B. & Simons, M., 2012. The potential for a very large earthquake along the southernmost Ryukyu subduction zone, *Geophys. Res. Lett.,* **39,** doi:10.1029/2012GL052764.

Huang, H.-H., Wu, Y.-M., Song, X., Chang, C.-H., Lee, S.-J., Chang, T.-M. & Hsieh, H.-H., 2013. Joint V_p and V_s tomography of Taiwan: Implications for subduction-collision orogeny, *Earth planet. Sci. Lett.,* submitted.

Kagan, Y.Y., 1991. 3-D rotation of double-couple earthquake sources, *Geophys. J. Int.,* **106,** 709–716.

Kanamori, H. & Rivera, L., 2008. Source inversion of W phase: speeding tsunami warning, *Geophys. J. Int.,* **175,** 222–238.

Kao, H. & Jian, P.-R., 2001. Seismogenic patterns in the Taiwan region: insights from source parameter inversion of BATS data, *Tectonophysics,* **333,** 179–198.

Kao, H., Jian, P.-R., Ma, K.-F., Huang, B.-S. & Liu, C.-C., 1998. Moment-tensor inversion for offshore earthquakes east of Taiwan and their implications to regional collision, *Geophys. Res. Lett.,* **25,** 3619–3622.

Kao, H., Liu, Y.-H., Liang, W.-T. & Chen, W.-P., 2002. Source parameters of regional earthquakes in Taiwan: 1999–2000 including the Chi-Chi earthquake sequence, *Terr. Atmos. Ocean. Sci.,* **13,** 279–298.

Kawakatsu, H., 1995. Automated near-realtime CMT inversion, *Geophys. Res. Lett.,* **22,** 2569–2572.

Kawakatsu, H., 1998. On the realtime monitoring of the long-period seismic wavefield, *Bull. Earthq. Res. Inst.,* **73,** 267–274.

Kubo, A., Fukuyama, E., Kawai, H. & Nonomura, K., 2002. NIED seismic moment tensor catalogue for regional earthquakes around Japan: quality test and application, *Tectonophysics,* **356,** 23–48.

Lee, S.-J., Huang, B.-S., Liang, W.-T. & Chen, K.-C., 2010. Grid-based moment tensor inversion technique by using 3-D Green's functions database: a demonstration of the 23 October 2004 Taipei earthquake, *Terr. Atmos. Ocean. Sci.,* **21,** 503–514.

Lee, S.-J., Liu, Q., Tromp, J., Komatitsch, D., Liang, W.-T. & Huang, B.-S., 2013. Toward real-time regional earthquake simulation II: real-time online earthquake simulation (ROS) of Taiwan earthquakes, *J. Asian Earth Sci.,* submitted.

Liang, W.-T., Liu, Y.-H. & Kao, H., 2003. Source parameters of regional earthquakes in Taiwan: January-December, 2001, *Terr. Atmos. Ocean. Sci.,* **14,** 249–260.

Liang, W.-T., Liu, Y.-H. & Kao, H., 2004. Source parameters of regional earthquakes in Taiwan: January-December, 2002, *Terr. Atmos. Ocean. Sci.,* **15,** 727–741.

Melgar, D., Bock, Y. & Crowell, B.W., 2011. Real-time moment tensor inversion and centroid location for large events from local and regional displacement records, in *Proceedings of the American Geophysical Union,* Fall Meeting 2011, Abstract #S51F-06.

Mellman, G.R., Burdick, L.J. & Helmberger, D.V., 1975. Determination of source parameters from body wave seismograms, *Earthq. Notes,* **40,** 44 pp.

Moore, G.E., 1965. Cramming more components onto integrated circuits, *Electronics,* **38,** 114–117.

Roumelioti, Z., Benetatos, C., Kiratzi, A. & Dreger, D., 2008. Near-real time moment tensors for earthquakes in Greece, Scientific Report, Department of Geophysics, Aristotle University of Thessaloniki (AUTH-solutions). Available at http://www.emsc-csem.org/Files/news/MISCELLANEOUS/Moment_tensors_EMSC_revised.pdf, last accessed 1st October 2013.

Saito, T. & Furumura, T., 2009. Three-dimensional tsunami generation simulation due to sea-bottom deformation and its interpretation based on the linear theory, *Geophys. J. Int.,* **178,** doi:10.1111/j.1365-246X.2009.04206.x.

Sipkin, S.A., 1982. Estimation of earthquake source parameters by the inversion of waveform data: synthetic waveforms, *Phys. Earth planet. Inter.,* **30,** 242–259.

Tajima, F., Mégnin, C.H., Dreger, D.S. & Romanowicz, B., 2002. Feasibility of real-time broadband waveform inversion for simultaneous moment tensor and centroid location determination, *Bull. seism. Soc. Am.,* **92,** 739–750.

Tsuruoka, H., Kawakatsu, H. & Urabe, T., 2009a. GRiD MT (grid-based real-time determination of moment tensor) monitoring the long-period seismic wavefield, *Phys Earth planet Inter.,* **175,** 8–16.

Tsuruoka, H., Rivera, L., Kawakatsu, H. & Kanamori, H., 2009b. Realtime source inversion using W-phase and GRiD MT for regional tsunami early warning, *Am. geophys. Un.,* S13A–1732.

Wallace, T.C., Helmberger, D.V. & Mellman, G.R., 1981. A technique for the inversion of regional data in source parameter studies, *J. geophys. Res.,* **86,** 1679–1685.

Zhu, L. & Rivera, L., 2001. Computation of dynamic and static displacement from a point source in multi-layered media, *Geophys. J Int.,* **148,** 619–627.